

Virtual probe stimulated tip-enhanced Raman spectroscopy: The extreme field enhancement in virtual-real probe dimer

Zhe Shen,^{1,a)} Xuefei Zi¹, Mengyuan Du¹, Lin Zhang¹, Yaochun Shen², and Maohai Hu¹

¹*School of Electronic and Optical Engineering, Nanjing University of Science and Technology, Nanjing 210094, China*

²*Department of Electrical Engineering & Electronics, University of Liverpool, Liverpool L69 3GJ, UK*

^{a)}shenzhe@njust.edu.cn

Abstract: Tip-enhanced Raman spectroscopy (TERS) can be used for scanning imaging, molecular detection and chemical analysis. The improvement of detection sensitivity, which is related to the electric field enhancement in the TERS substrate, has attracted much attentions from researchers. In this work, we numerically studied the local electric field enhancement in the virtual-real probe dimer structure with a vertical gap. We mainly analyzed the influence of the structure parameters on the field enhancement using the finite-difference time-domain (FDTD) method. The Raman enhancement factor could reach up to 1.6×10^{15} . The local field enhancement benefits from plasmon hybridization between the longitudinal component of the virtual probe (VP) and the local surface plasmon (LSP) of the real probe. We also found that the FWHM of the electric field was as narrow as 7.8 nm and the volume of the hotspot for single-molecule detection can reach a maximum value of 155 nm^3 . The virtual-real probe dimer structure has ultrahigh field enhancement and spatial resolution, which is promising for high-sensitivity detection and high-resolution imaging.

I. Introduction

Raman detection is a fast, non-destructive modern characterization technique that provides molecular vibration information¹, but the Raman scattering is a fast and inelastic energy exchange process with 10^{-6} - 10^{-8} photons of the incident light within a picosecond or less, leading to a weak Raman scattering signal². Surface-enhanced Raman scattering (SERS) can significantly increase the Raman signals of the analyte with an average enhancement factor of about 10^4 - 10^6 by placing it near the surface of the metal nanostructured substrate¹. For the conventional SERS substrates including metal nanoparticles^{3,4} and metal nanoshells⁴, moderately enhanced electric fields can be formed on their surfaces. For nanostructures with sharp corners, including metal nanocubes⁵, gold nanostars⁶, and metal probe⁷, the electric field enhancement is stronger than those nanostructures with smooth surfaces, because the electric fields could be more highly localized at the vicinity of the structure apices. To further enhance the electric field, Lu *et al.* proposed a method to acquire a considerable field enhancement by illuminating the metal probe with focused multi-order radially polarized beam (RPB)⁸. However, the above-mentioned field enhancement is mainly attributed to the local surface plasmons resonance (LSPR) of the monomer structure, resulting in a limited enhancement.

In recent years, coupled metal nanostructures with gaps have attracted much attention³. The standard coupled structures, including nanoparticle dimer⁴, bowtie⁹ and its array pattern¹⁰, *etc.*, can be used to obtain a Raman enhancement factor of about 6 orders of magnitude, which is much higher than that of the monomer structure. The huge field enhancement comes from the plasmonic interaction in the nanogap. Following this mechanism, the coupled structure with the metal probe has been studied. Zhang *et al* have obtained the Raman enhancement factor of about 14 orders of magnitude by a concurrent scanning double-tip-enhanced Raman scattering (CS-TERS) system¹¹. Nevertheless, the utilized coupled structure is horizontally-oriented, thus providing no scanning ability. Also, the introduction of an extra tip structure would add extra cost and complexity to the device. Sun *et al.* found that the electric field enhancement of the longitudinal orientation coupled structure comprised of a probe and a gold nanoparticle was larger than that of the monomer probe¹². Although this configuration has scanning ability, the instability of the nanoparticle will affect the field enhancement. A vertically-oriented coupled structure comprised of double probes is expected to achieve higher field enhancement with the scanning function, but the potential disadvantage of this structure is the requirement for the precise alignment of the double probes.

As a counterpart of the real probe, virtual probe (VP)¹³⁻¹⁵ has been proposed and used to achieve the enhancement of Raman signal and dynamic detection with high spatial resolution¹⁵. It is a standing wave generated by the constructive interference of the surface plasmon waves on a flat metal film. The longitudinal component is dominant in its electric field^{14,15}. It has been demonstrated that a vertical coupled structure comprised of the VP and metal nanoparticle can be used to achieve an ultrahigh electric field enhancement^{14,16}, enabling single-molecule detection. Nevertheless, the instability of the nanoparticle restricts its practical application.

Here, a virtual-real probe dimer structure with a vertical gap was used to enhance the electric field and was simulated using the finite-difference time-domain (FDTD) method. We investigated the influence of the following parameters on the electric field enhancement: the curvature radius R of the real probe, the longitudinal gap distance d between the metal probe and metal substrate, and the excitation laser wavelength λ . Furthermore, we also studied the spatial resolution and hotspot volume of the structure.

II. Theory and method

A. The generation of virtual probe by focused radially polarized beam

The schematic diagram of the virtual-real probe dimer is shown in Fig. 1(a). The coupled structure is illuminated by the focused RPB from bottom to up, which has covered the specific angle of the wave vector matching for the excitation of surface plasmon resonance (SPR)^{17,18}. The laser wavelength is 632.8 nm. The real silver probe is modeled as an inverted cone with an angle of 45° combining with a hemisphere at the end. The optical constant of silver follows the Johnson-Christy model¹⁹. Due

to the sensitivity of surface plasmon to the TM polarization, the excited surface plasmon polaritons have a symmetrical circle distribution on the metal surface, as shown in Fig. 1(a). When surface plasmon waves propagate towards the center, due to the constructive interference of the surface plasmon waves, a strong standing wave field is formed at the central area, as shown in Fig. 1(b), also called virtual probe^{13,14}.

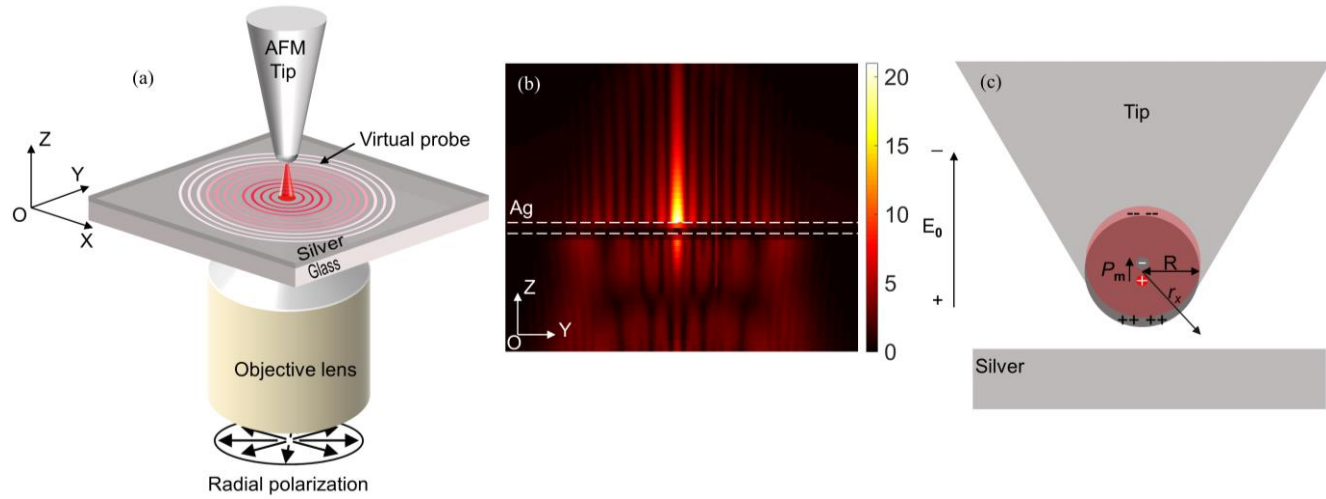


FIG. 1. (a) Schematic of the virtual-real probe dimer. (b) The local electric field distribution of the VP in the Y-Z section. (c) Schematic of a physical model for the virtual-real probe dimer.

To calculate the electric field distribution of VP, we only consider the longitudinal component of VP, which dominates the total field distribution²⁰. According to the Richards-Wolf vector diffraction theory, the longitudinal component can be expressed as^{20,21}

$$E_z(r, \varphi, z) = i2A \int_0^{\theta_{\max}} \cos^{1/2}(\theta) P(\theta) t_p(\theta) \sin^2 \theta J_0(k_1 r \sin \theta) \exp\left[iz(k_2^2 - k_1^2 \sin^2 \theta)^{1/2}\right] d\theta, \quad (1)$$

where $t_p(\theta)$ is TM polarization transmission coefficient with incident angle θ , A is a constant, $P(\theta)$ is the pupil apodization function, $J_m(x)$ is the first kind of m -order Bessel function, θ_{\max} is the maximum incident angle with focused RPB, k_1 and k_2 are the wave vectors above and below the silver layer, respectively.

The virtual-real probe dimer can be considered as a VP stimulated tip-enhanced Raman scattering (TERS) structure, to analyze the local electric field, the tip of the metal probe is regarded as a sphere as shown in Fig. 1(c), and VP is regarded as an incident source. By using the dipole approximation theory^{14,22}, the polarizability of the metal sphere with radius R is $\alpha_m = 4\pi\epsilon_0 R^3 \frac{\epsilon_m - 1}{\epsilon_m + 2}$, where ϵ_0 and ϵ_m are the dielectric constants of the vacuum and metal sphere, respectively. The dipole

moment of the metal sphere is related to the incident electric field \mathbf{E}_0 : $\mathbf{P}_m = \alpha_m \mathbf{E}_{inc}$ ^{14,22}. The local electric field around the metal sphere at the position of \mathbf{r}_x is²³:

$$\mathbf{E}_{loc} = \mathbf{E}_0 + \left(\frac{R}{|\mathbf{r}_x|} \right)^3 [3\mathbf{n} \cdot (\mathbf{n} \cdot \mathbf{E}_0) - \mathbf{E}_0] \quad (2)$$

where \mathbf{n} represents a unit vector along the direction of \mathbf{E}_0 .

III. Results and Discussions

A. The field enhancement in the virtual-real VP dimer

To compare the electric field enhancement of the coupled structure with and without VP, we simulated the local electric field distributions of Ag probe-glass, Ag probe-VP, and Ag-coated probe-VP configurations. We adopted the perfect match layer (PML) boundary conditions in all our simulations. The gap distance d was set as 2 nm and the curvature radius R of the hemisphere within the metal probe was set as 15 nm. For enhancing computational accuracy whilst reducing computing resources, we used non-uniform mesh, the Yee cell sizes in the plasmonic nanogap region were set as $1 \times 1 \times 1 \text{ nm}^3$. Figs. 2(a)-(c) show the local electric field intensity with logarithmic scale of different vertical coupled structures. Based on the local electric field, we can obtain the electric field enhancement factor according to the formula $M = |\mathbf{E}_{loc} / \mathbf{E}_{inc}|$, where \mathbf{E}_{inc} represents the incident electric field²⁴. Since the Raman enhancement is proportional to the fourth power of the local electric field enhancement²⁵, the Raman enhancement factor can be presented as M^4 . For the Ag probe-glass configuration shown in Fig. 2(a), the field enhancement originates from the LSPR of the Ag probe, the maximal M is about 26.3 and the Raman enhancement factor reaches up to 4.8×10^5 . For the Ag probe-VP configuration shown in Fig. 2(b), the field enhancement benefits from the plasmonic interaction¹⁴ between the Ag probe and VP, the maximal M reaches up to 915.8 and the Raman enhancement factor reaches up to 7.0×10^{11} . Considering the probe used in practical applications, we performed the simulation of an Ag-coated probe shown in Fig. 2(c), the silver coating thickness is 40 nm. The maximal M reaches up to 906.0 and the Raman enhancement factor reaches up to 6.7×10^{11} . Through the comparison of the local field enhancement of the configurations with or without VP, we can conclude that VP stimulated real probe structure can effectively improve the field enhancement.

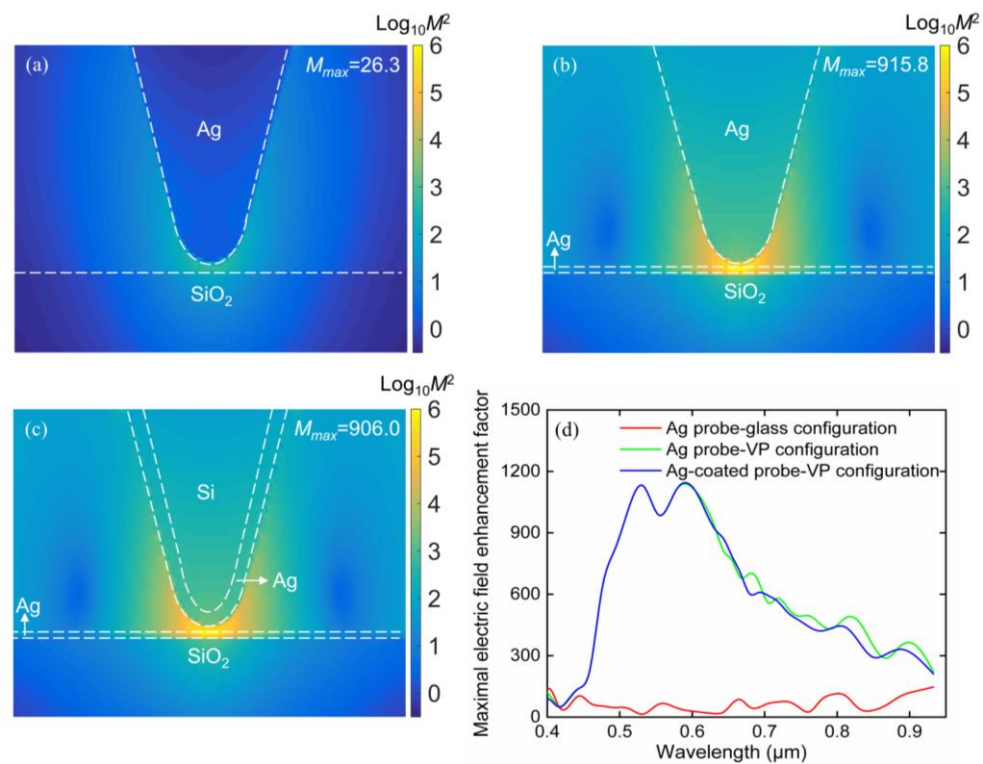


FIG. 2. Local electric field intensity with logarithmic scale in (a) Ag probe-glass, (b) Ag probe-VP, and (c) Ag-coated probe-VP configurations. (d) The spectra responses of different configurations.

We also calculated the spectra responses of different configurations with wavelength ranging from 0.4 μm to 0.9 μm , as shown in Fig. 2(d). The Ag probe-glass coupled structure shows a weak hybridization effect in the wavelength range, resulting in a smaller M and its maximum value is about 85.9. The Ag probe-VP and Ag-coated probe-VP configurations have maximum electric field enhancement factors of 1131.0 and 1125.9, respectively. This reveals that the VP engaged configuration can produce a larger field enhancement and over a wide spectral range. The curve of Ag-coated probe-VP configuration almost overlaps with that of Ag probe-VP configuration especially in the wavelength range from 0.4 μm to 0.6 μm , this means the Ag probe can be replaced by the Ag-coated probe in the TERS application.

B. Gap distance and curvature radius dependent field enhancement

For the traditional dimer structure, the electric field enhancement is related to the dimer gap distance. Here we further investigated the influence of the gap distance d in the virtual-real probe dimer structure on the field enhancement. As shown in Fig. 3(a), the electric field enhancement factor decays with the gap distance d increasing from 2 nm to 10 nm. According to Eq. (2), \mathbf{E}_{loc} is positively related with \mathbf{E}_0 . If we assume the virtual probe as the incident electric field (\mathbf{E}_0). Since the longitudinal component of VP decays exponentially along the longitudinal direction^{20,21}, which can be explained according to the exponential term in Eq. (1), we can obtain that \mathbf{E}_{loc} decays exponentially with the increasing of the gap distance d .

Through the comparison between theoretical analysis and simulation result, we can conclude that the local field enhancement is exponential dependence on d . When d is 2 nm, the field enhancement factor is more than 10^3 in the wavelength range of 0.5 μm to 0.6 μm , which is enough for single-molecule detection. The result that the SPR peak blue shifts with the increase of the gap distance is consistent with the previous study²⁶.

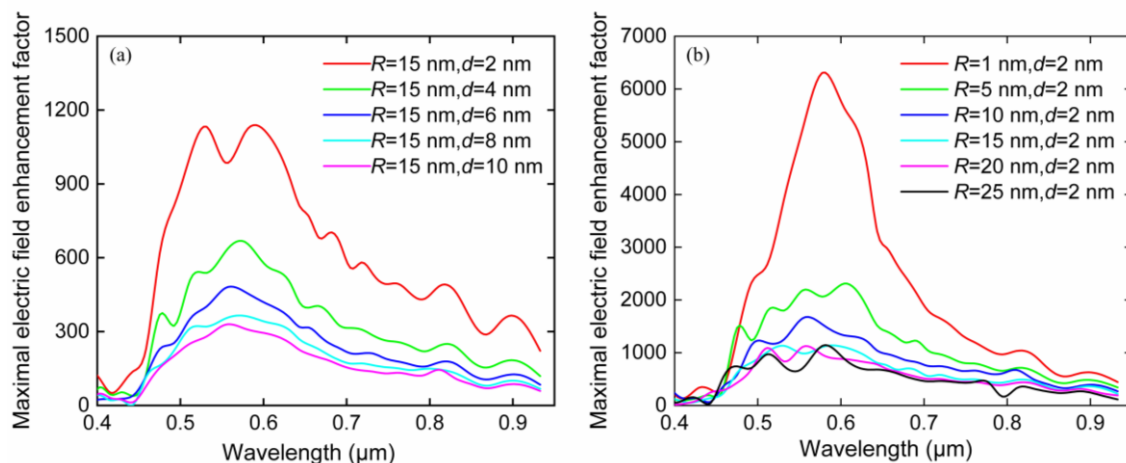


FIG. 3. The maximum electric field enhancement factor of the virtual-real probe dimers with different parameters in the wavelength range from 0.3 μm to 0.9 μm . (a) The electric field enhancement with the variation of d every 2 nm when R is 15 nm. (b) The field enhancement with the variation of R every 5 nm when d is 2 nm. In the calculations, the cone angle θ is fixed to be 45° .

In order to study the edge effect of the real probe on the electric field enhancement, we simulated the Ag probe-VP configuration. The gap distance d is selected as 2 nm with a moderate enhancement. As we can see in Fig. 3(b), the field enhancement decreases when the curvature radius R increases from 1 nm to 25 nm. A smaller curvature radius leads to a remarkable field enhancement due to the lightning-rod effect that a large amount of charge accumulates on the Ag probe apex²⁷. We can find that when the curvature radius ranges from 1 nm to 25 nm, the electric field enhancement factor can exceed 10^3 , which provides high enough enhancement for single-molecule detection. In particular, the field enhancement factor reaches a significant value of 6.3×10^3 in the condition $R = 1$ nm and $d = 2$ nm, and the Raman enhancement factor reaches up to 1.6×10^{15} .

C. Curvature radius dependent spatial resolution and hotspot region

Because the spatial resolution is another important performance parameter of the Raman imaging and detection system, we studied the effect of the curvature radius on the spatial resolution, which is defined as the FWHM of the confined electric field, i.e., the hotspot. The FWHM of the hotspot increases from 7.8 nm to 17.6 nm when the curvature radius increases from 5 nm to 25 nm. It can be also found that the FWHMs of the confined electric fields are always smaller than or close to the curvature radius, this is consistent with the report in reference²⁷. The electric field and spatial resolution can be improved by

optimizing the curvature radius^{24,28,29}. Therefore, a sharper probe will not only excite a stronger local electric field but also lead to a higher spatial resolution.

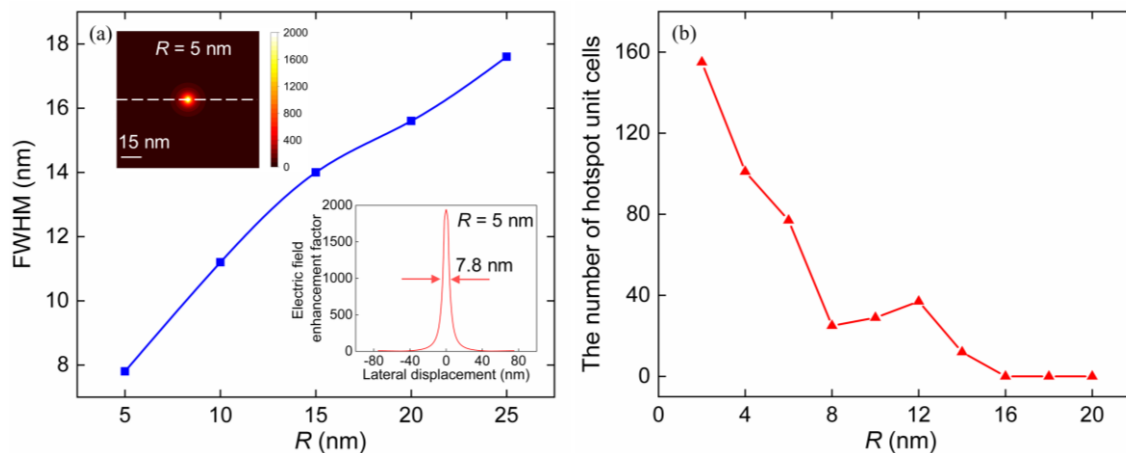


FIG. 4. (a) The FWHM with the variation of R . The insets in the top-left and bottom-right corners represent the local electric field distribution of the hotspot ($R = 5$ nm) and the FWHM along the dotted white line direction, respectively. (b) The number of hotspot unit cells with the variation of R .

In order to quantify the single-molecule detection volume of the virtual-real probe dimer structure for Raman detection applications, we counted the number of the Yee cells whose electric field enhancement factor is larger than 10^3 in the plasmonic nanogap region, which were called hotspot unit cells here. As the curvature radius increases, the number of hotspot unit cells generally shows a decreasing trend except for the special R of 10 nm and 12 nm in Fig. 4(b). The electric field enhancement decreases slowly with the increasing of the curvature radius, but the scattering cross-section of the tip apex increases gradually with increasing R . That is the reason why the number of the hotspot unit cells increased slightly with varying R from 8 nm to 12 nm. When R is 2 nm, the number of hotspot unit cells reaches the maximum value of 155. The results demonstrate that the virtual-real probe dimer has the ability to detect single molecule within a certain spatial volume.

D. The Raman enhancement in coupled substrates

Finally, we have summarized the Raman enhancement factors of several typical coupled structures of SERS and TERS, as shown in Fig. 5. For traditional nanoparticle dimers^{4,30}, when the interparticle axis is perpendicular to the incident polarization, the Raman enhancement factor is only 2.6×10^2 , whilst the interparticle axis is parallel to the incident polarization, the Raman enhancement factor reaches up to 3.4×10^6 . For the sphere-film coupled structure with side illumination³, the single sphere structure with bottom illumination³¹, and the tip-sphere coupled structure with side illumination^{12,24}, the Raman enhancement factors can reach 4.3×10^4 , 5.6×10^3 , and 1.8×10^{10} , respectively. For the tip-film coupled structure with side illumination²⁴, the tip structure with RPB illumination from bottom⁸, and the tip-tip coupled structure¹¹, the Raman enhancement factors can

reach 1.5×10^{10} , 1.7×10^{10} , and 1.6×10^{14} , respectively. These results reveal that the traditional coupled structures with tips are over that with spheres in terms of electric field enhancement. This is because the tip has the lightning-rod effect resulting in a remarkable field enhancement. The Raman enhancement factor of focused RPB excited VP on the metal film¹⁴ is about 1.3×10^7 . The plasmonic interaction between the VP and the LSP of the metal sphere in the sphere-VP coupled structure leads to the Raman enhancement factor with a value of 1.6×10^{13} , which is able to detect single molecule¹⁴. Given the lightning-rod effect of the tip, the tip-VP coupled structure, i.e., the virtual-real probe dimer, has generated a significant TERS enhancement factor with a value of 1.6×10^{15} , which is highest for the existing SERS substrates to our best knowledge.

Incidence	Typical M^4	Sphere	Tip	Metal film	RPB	VP	
Combination [Ref.]							
Sphere		2.6×10^2 3.4×10^6 [4,30]		1.8×10^{10} 1.6×10^{14} [12,24]	4.3×10^4 1.5×10^{10} [3]	5.6×10^3 1.7×10^{10} [31]	1.6×10^{13} 1.6×10^{15} [14]
Tip		1.8×10^{10} [12,24]	1.6×10^{14} [11]	1.5×10^{10} [24]	1.7×10^{10} [8]	1.3×10^7 [14]	
Metal film		4.3×10^4 [3]					
RPB		5.6×10^3 [31]	1.7×10^{10} [8]	1.3×10^7 [14]			
VP		1.6×10^{13} [14]	1.6×10^{15}				

FIG. 5. The enhancement effect of different coupled structures. The top-left, top-right, and bottom areas of the top-left insert of the table represent the light source incident direction, the typical Raman enhancement (M^4), and different coupled structures, respectively. M^4 of tip-VP coupled structure in this work is marked by red.

IV. Conclusion

In summary, we have demonstrated that the vertically-oriented virtual-real probe dimer provides not only an ultrahigh electric field enhancement but also a high spatial resolution in the nanometer range. VP is responsible for high field enhancement as our structure can be comprehended as a VP stimulated TERS. Our simulation results using the dipole approximation theory shown that the electric field enhancement factor is dependent on the curvature radius R of the real probe, the longitudinal gap distance d , and the excitation laser wavelength λ . By optimizing these parameters, the Raman enhancement factor of the vertically-oriented virtual-real probe dimer could reach as high as 1.6×10^{15} and the FWHM of the electric field

is as small as 7.8 nm. Through the calculation of the number of the hotspot unit cells, it was found that the space single-molecule detection volume in our structure can be 155 nm^3 . The temperature at the gap area can be controlled within a proper range by limiting the incident light power (see part 1 in the supplementary material) so that most biological samples will not be damaged at low temperatures. When a position deviation occurs in our coupled structure, the field enhancement shows a robust character (see part 2 in the supplementary material), which revealed that our structure has no alignment issue. Therefore, our model has great potential in scanning imaging and single-molecule detection.

Supplementary material

See the supplementary material for thermal calculation of virtual-real probe dimer and the calculation of electric field enhancement in the dimer with the deviation between the virtual-real probes.

Acknowledgments

This work is supported by National Natural Science Foundation of China (NSFC) (61805119), Natural Science Foundation of Jiangsu Province (BK20180469), and The Fundamental Research Funds for the Central Universities (30919011275). The authors thank Dr. Yikai Chen for the valuable discussions.

Data availability

The data that supports the findings of this study are available within the article and its supplementary material.

References

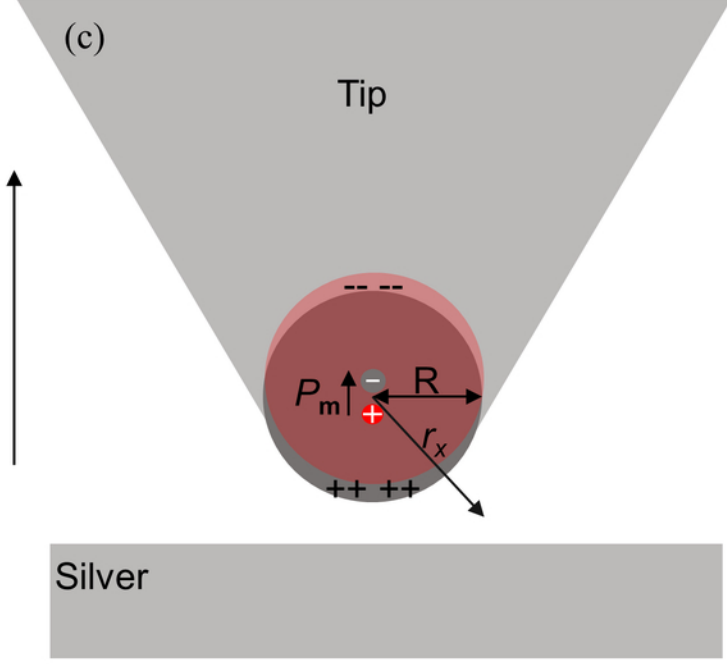
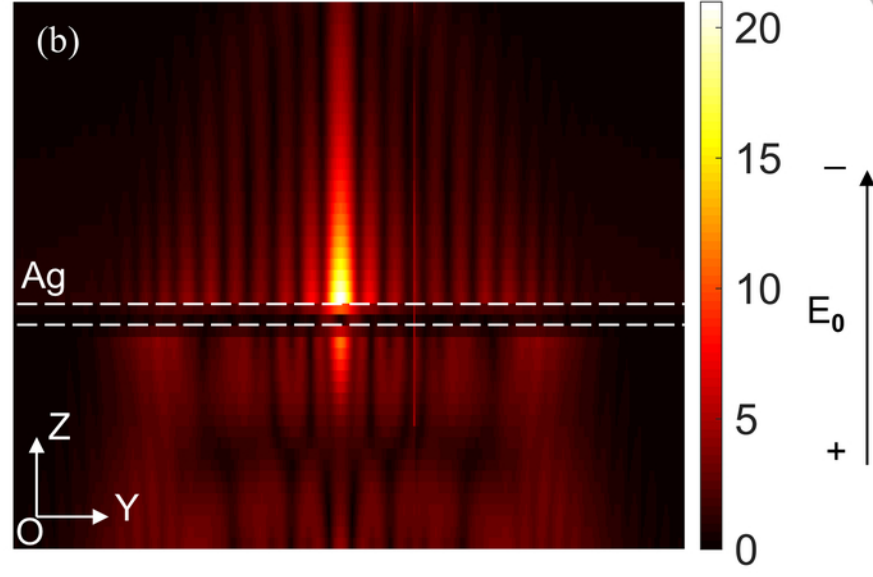
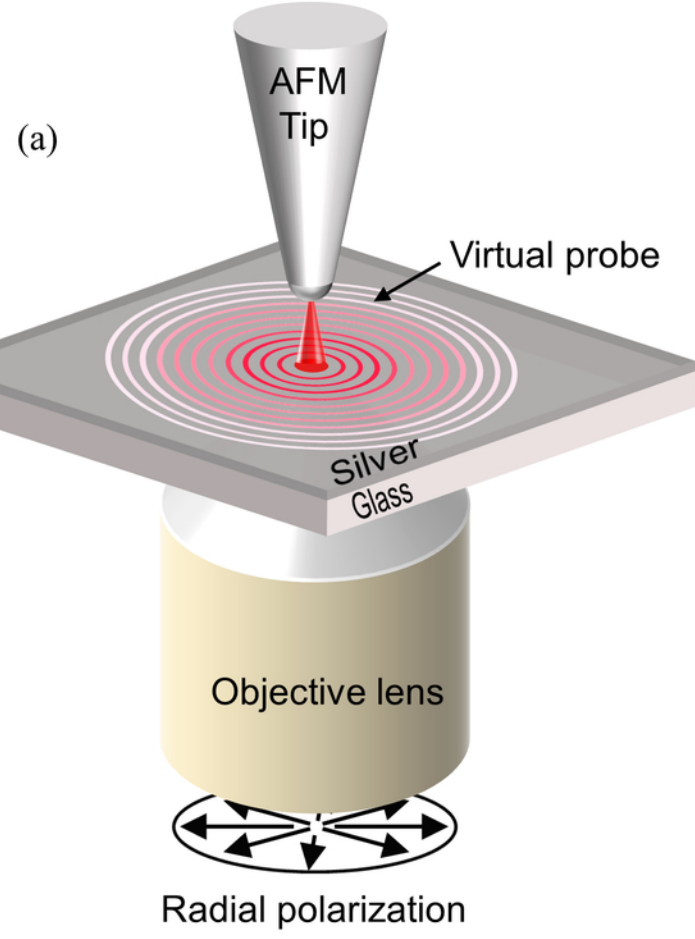
- ¹M. Prochazka, *Surface-Enhanced Raman Spectroscopy* (Springer International Publishing, New York, 2016), p. 9.
- ²F. Shao and R. Zenobi, *Anal. Bioanal. Chem.* **411**, 37 (2019).
- ³S. Y. Ding, J. Yi, J. F. Li, B. Ren, D. Y. Wu, R. Panneerselvam, and Z. Q. Tian, *Nat. Rev. Mater.* **16**, 1 (2016).
- ⁴C. E. Talley, J. B. Jackson, C. Oubre, N. K. Grady, C. W. Hollars, S. M. Lane, T. R. Huser, P. Nordlander, and N. J. Halas, *Nano Lett.* **5**, 1569 (2005).
- ⁵J. M. McLellan, Z. Y. Li, A. R. Siekkinen, and Y. N. Xia, *Nano Lett.* **7**, 1013 (2007).
- ⁶C. G. Khoury and T. Vo-Dinh, *J. Phys. Chem. C* **112**, 18849 (2008).
- ⁷N. Hayazawa, Y. Inouye, Z. Sekkat, and S. Kawata, *Opt. Commun.* **183**, 333 (2000).
- ⁸C. Lu, P. Tang, X. Lu, Q. Zhang, S. Liu, J. Tian, and L. Zhong, *Plasmonics* **13**, 1881 (2018).
- ⁹N. A. Hatab, C. H. Hsueh, A. L. Gaddis, S. T. Retterer, J. H. Li, G. Eres, Z. Zhang, and B. Gu, *Nano Lett.* **10**, 4952 (2010).
- ¹⁰J. Zhang, M. Irannejad, and B. Cui, *Plasmonics* **10**, 831 (2014).
- ¹¹Q. Zhang, X. Lu, Y. Yuan, D. Zhang, J. Li, and L. Zhong, *Plasmonics* **11**, 247 (2015).
- ¹²M. Sun, Y. Fang, Z. Yang, and H. Xu, *Phys. Chem. Chem. Phys.* **11**, 9412 (2009).
- ¹³N. Hayazawa, H. Ishitobi, A. Taguchi, A. Tarun, K. Ikeda, and S. Kawata, *Jpn. J. Appl. Phys.* **46**, 7995 (2007).
- ¹⁴Z. Shen, L. Su, and Y. C. Shen, *Opt. Express* **24**, 16052 (2016).
- ¹⁵Q. Sun, Y. Zhang, L. Sun, Y. Yang, C. Min, S. Zhu, and X. Yuan, *Opt. Commun.* **392**, 64 (2017).
- ¹⁶L. Du, G. Yuan, D. Tang, and X. Yuan, *Plasmonics* **6**, 651 (2011).
- ¹⁷H. Kano, S. Mizuguchi, and S. Kawata, *J. Opt. Soc. Am. B.* **15**, 1381 (1998).
- ¹⁸K. J. Moh, X. C. Yuan, J. Bu, S. W. Zhu, and B. Z. Gao, *Opt. Lett.* **34**, 971 (2009).
- ¹⁹P. B. Johnson and R. W. Christy, *Phys. Rev. B* **6**, 4370 (1972).
- ²⁰Q. W. Zhan, *Opt. Lett.* **31**, 1726 (2006).
- ²¹B. Richards, E. Wolf, and D. Gabor, *Proc. R. Soc., Lond., A*, **253**, 358 (1959).
- ²²L. Novotny and B. Hecht, *Principles of Nano-Optics* (Cambridge University Press, Cambridge, 2006), p. 154.
- ²³M. Richard-Lacroix, Y. Zhang, Z. Dong, and V. Deckert, *Chem. Soc. Rev.* **46**, 3922 (2017).

This is the author's peer reviewed, accepted manuscript. However, the online version of record will be different from this version once it has been copyedited and typeset.

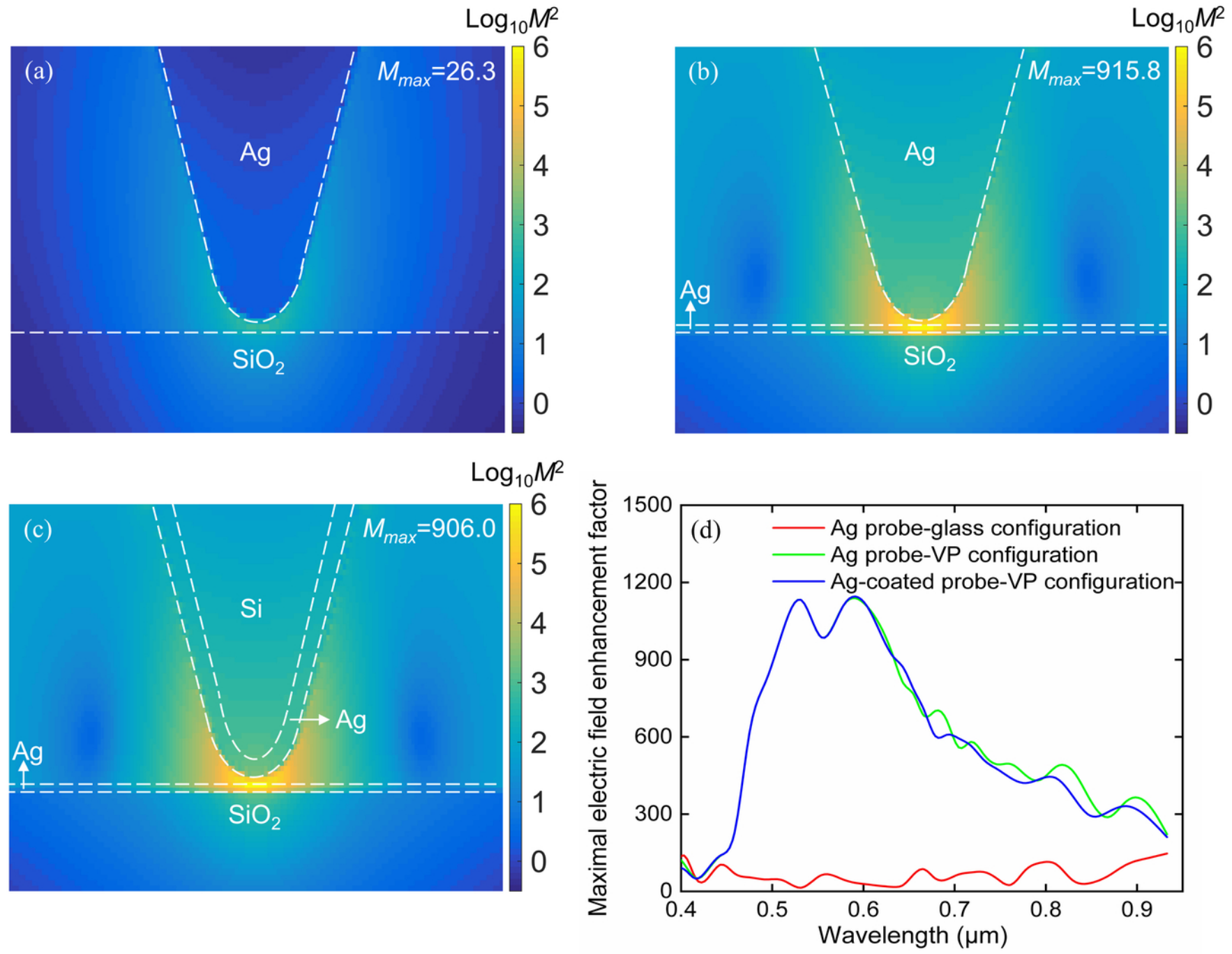
PLEASE CITE THIS ARTICLE AS DOI: 10.1063/5.0046647

- ²⁴Z. Yang, J. Aizpurua, and H. Xu, *J. Raman Spectrosc.* **40**, 1343 (2009).
- ²⁵R. Pilot, R. Signorini, C. Durante, L. Orian, M. Bhamidipati, and L. Fabris, *Biosensors-Basel* **9**, 8 (2019).
- ²⁶A. L. Demming, F. Festy, and D. Richards, *J. Chem. Phys.* **122**, 184716 (2005).
- ²⁷T. X. Huang, S. C. Huang, M. H. Li, Z. C. Zeng, X. Wang, and B. Ren, *Anal. Bioanal. Chem.* **407**, 8177 (2015).
- ²⁸L. Meng, T. Huang, X. Wang, S. Chen, Z. Yang, and B. Ren, *Opt. Express* **23**, 13804 (2015).
- ²⁹H. Chen, Y. Zhang, Y. Dai, C. Min, S. Zhu, and X. Yuan, *Photonics Res.* **8**, 103 (2020).
- ³⁰E. Hao and G. C. Schatz, *J. Chem. Phys.* **120**, 357 (2004).
- ³¹K. Sendur and A. Sahinoz, *Opt. Express* **17**, 10910 (2009).

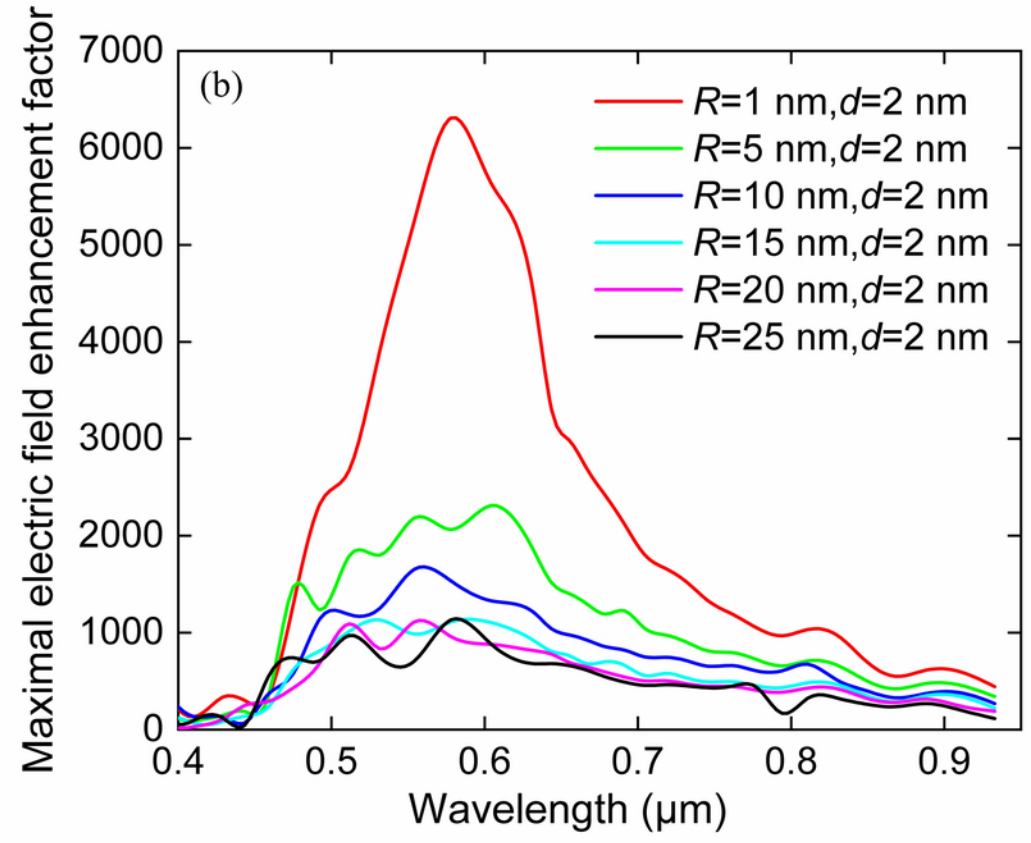
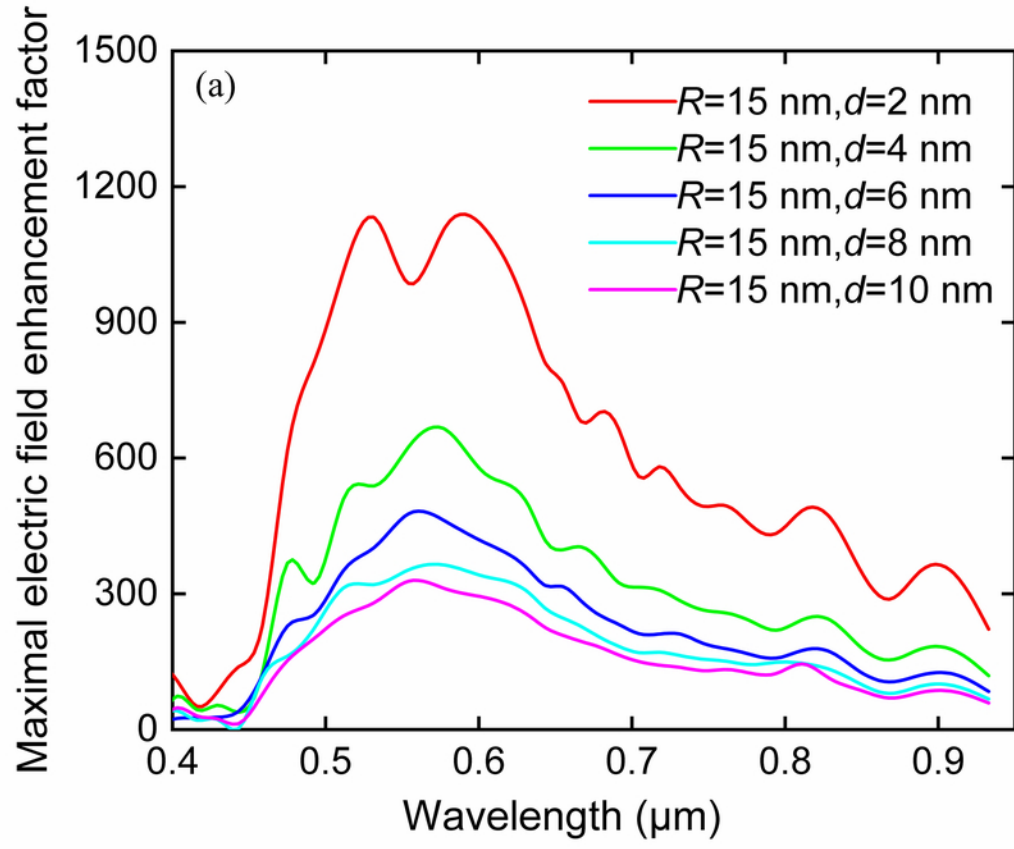
This is the author's peer reviewed, accepted manuscript. However, the online version of record will be different from this version once it has been copyedited and typeset.
PLEASE CITE THIS ARTICLE AS DOI: 10.1063/5.0046647



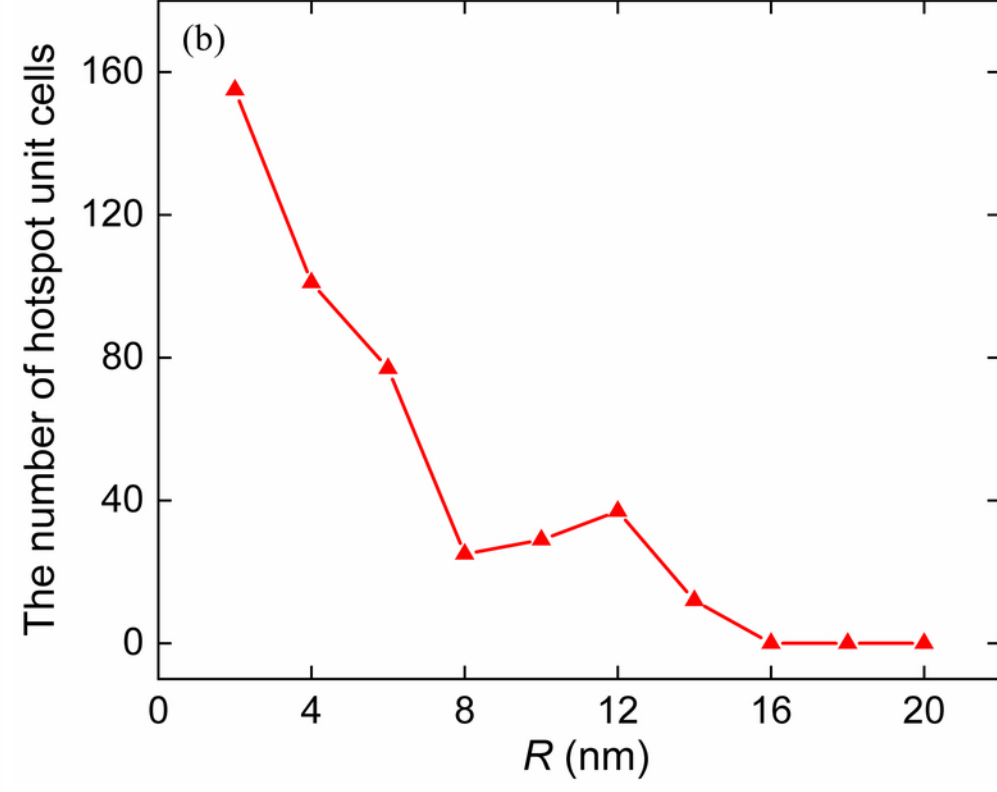
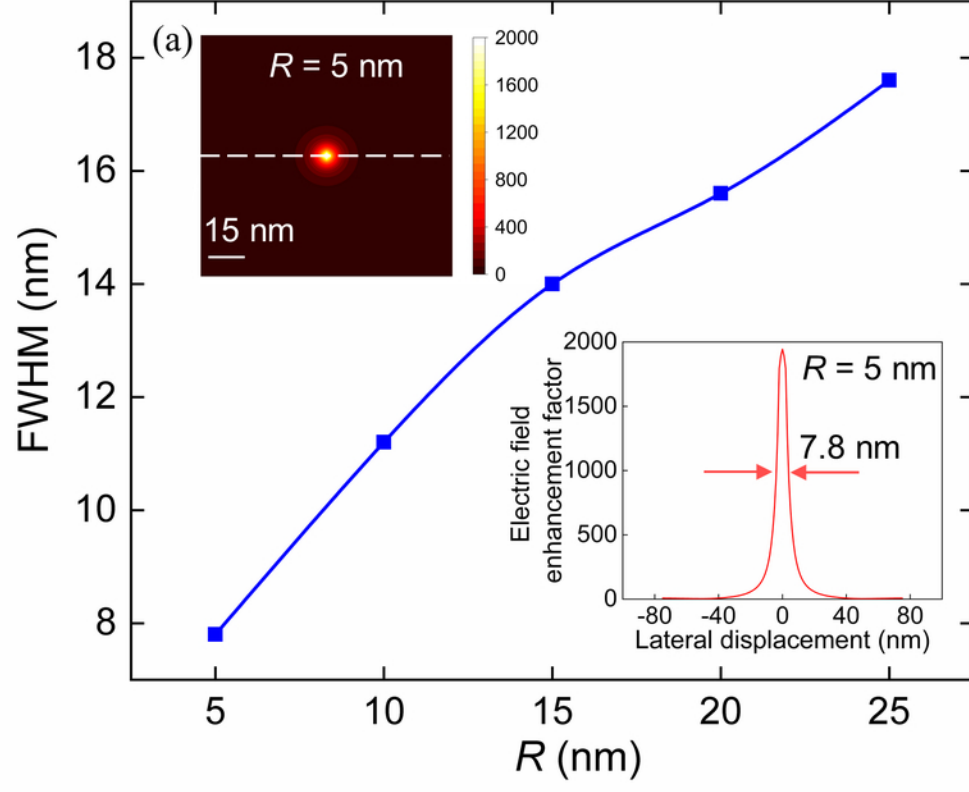
This is the author's peer reviewed, accepted manuscript. However, the online version of record will be different from this version once it has been copyedited and typeset.
PLEASE CITE THIS ARTICLE AS DOI: 10.1063/5.0046647




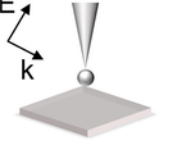
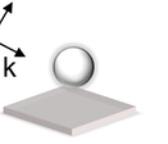
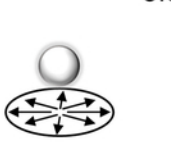
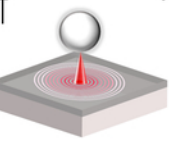
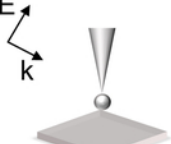
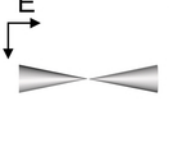
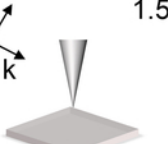
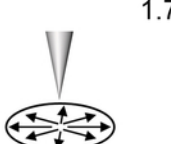
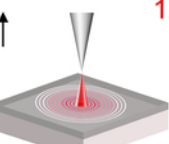
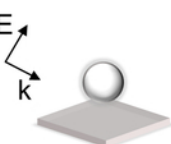
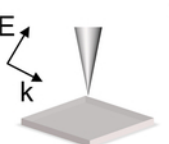
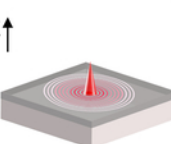
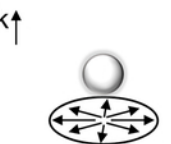
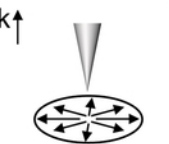
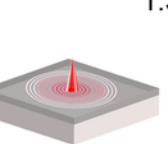
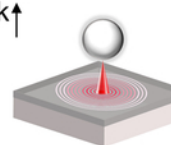
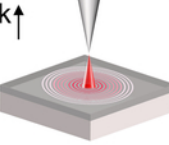
This is the author's peer reviewed, accepted manuscript. However, the online version of record will be different from this version once it has been copyedited and typeset.
PLEASE CITE THIS ARTICLE AS DOI: 10.1063/5.0046647



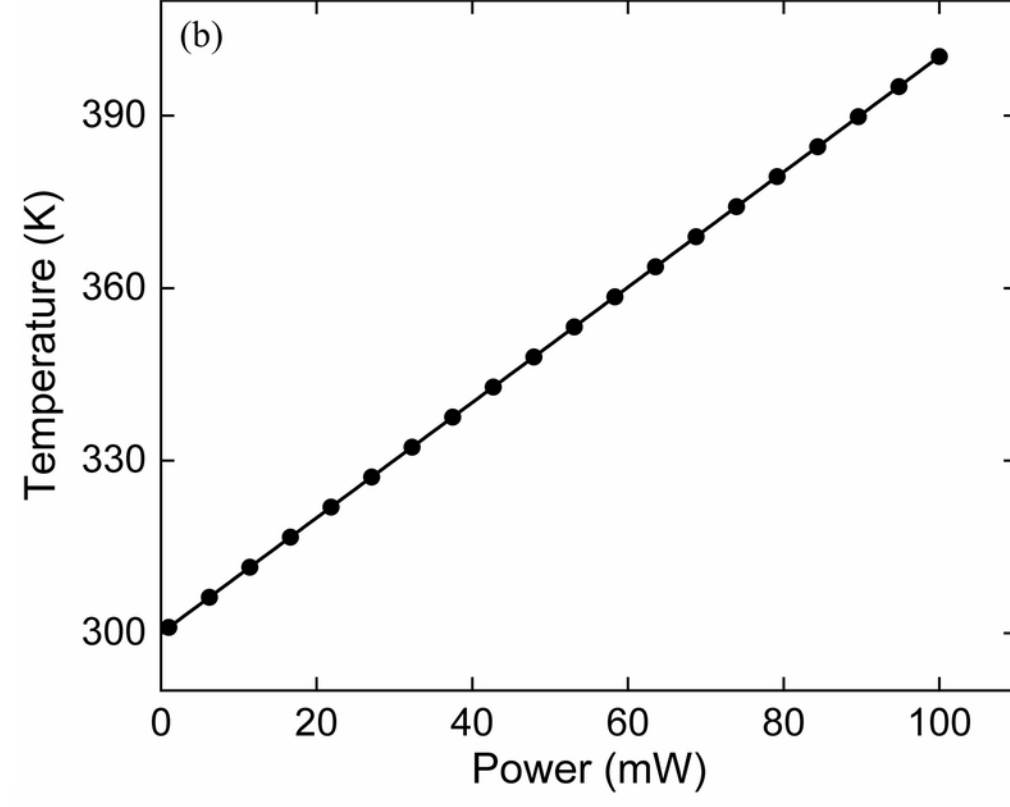
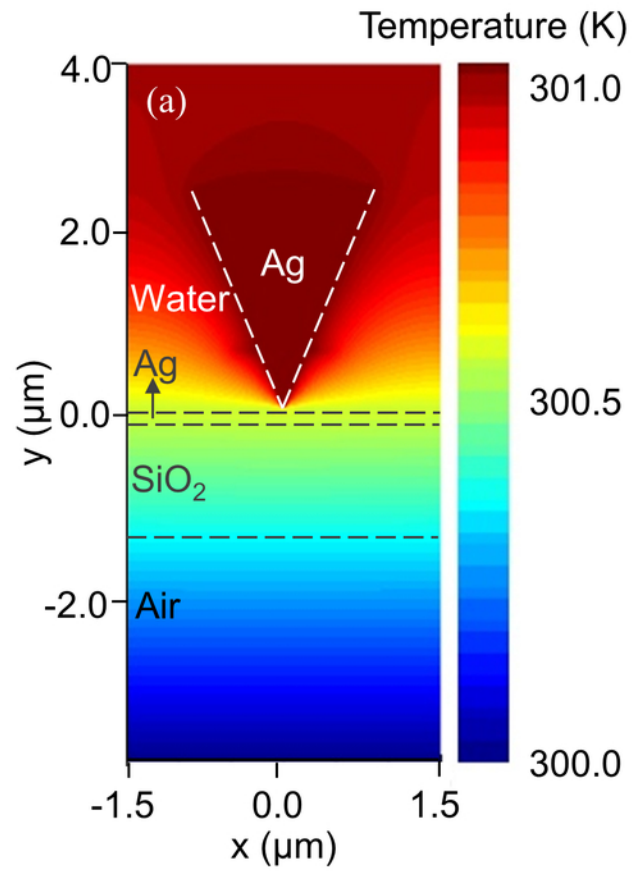
This is the author's peer reviewed, accepted manuscript. However, the online version of record will be different from this version once it has been copyedited and typeset.
PLEASE CITE THIS ARTICLE AS DOI: 10.1063/5.0046647



This is the author's peer reviewed, accepted manuscript. However, the online version of record will be different from this version once it has been copyedited and typeset.
PLEASE CITE THIS ARTICLE AS DOI: 10.1063/5.0046647

Incidence	Typical M^4	Sphere	Tip	Metal film	RPB	VP
Combination [Ref.]						
Sphere	 Sphere 2.6×10^2 3.4×10^6 [4,30]	 Tip 1.8×10^{10} [12,24]	 Metal film 4.3×10^4 [3]	 RPB 5.6×10^3 [31]	 VP 1.6×10^{13} [14]	
Tip	 Tip 1.8×10^{10} [12,24]	 Metal film 1.6×10^{14} [11]	 RPB 1.5×10^{10} [24]	 VP 1.7×10^{10} [8]	 VP 1.6×10^{15}	
Metal film	 Metal film 4.3×10^4 [3]	 Metal film 1.5×10^{10} [24]		 RPB 1.3×10^7 [14]		
RPB	 RPB 5.6×10^3 [31]	 RPB 1.7×10^{10} [8]	 VP 1.3×10^7 [14]			
VP	 VP 1.6×10^{13} [14]	 VP 1.6×10^{15}				

This is the author's peer reviewed, accepted manuscript. However, the online version of record will be different from this version once it has been copyedited and typeset.
PLEASE CITE THIS ARTICLE AS DOI: 10.1063/5.0046647



This is the author's peer reviewed, accepted manuscript. However, the online version of record will be different from this version once it has been copyedited and typeset.
PLEASE CITE THIS ARTICLE AS DOI: 10.1063/5.0046647

